


**Tracer diffusion in crowded solutions of sticky polymers**T. P. O. Nogueira <sup>\*</sup>*Departamento de Física, Instituto de Física e Matemática, Universidade Federal de Pelotas. Caixa Postal 354, 96001-970, Pelotas, Brazil*H. O. Frota <sup>†</sup>*Department of Physics, Federal University of Amazonas, 69077-000 Manaus, AM, Brazil*Francesco Piazza <sup>‡</sup>*Université d'Orléans, Centre de Biophysique Moléculaire (CBM), CNRS UPR4301, Rue C. Sadron, 45071 Orlans, France*José Rafael Bordin <sup>§</sup>*Departamento de Física, Instituto de Física e Matemática, Universidade Federal de Pelotas. Caixa Postal 354, 96001-970, Pelotas, Brazil*

(Received 29 June 2020; accepted 14 September 2020; published 29 September 2020)

Macromolecular diffusion in strongly confined geometries and crowded environments is still to a large extent an open subject in soft matter physics and biology. In this paper, we employ large-scale Langevin dynamics simulations to investigate how the diffusion of a tracer is influenced by the combined action of excluded-volume and weak attractive crowder-tracer interactions. We consider two species of tracers, standard hard-core particles described by the Weeks-Chandler-Andersen (WCA) repulsive potential and core-softened (CS) particles, which model, e.g., globular proteins, charged colloids, and nanoparticles covered by polymeric brushes. These systems are characterized by the presence of two length scales in the interaction and can show waterlike anomalies in their diffusion, stemming from the inherent competition between different length scales. Here we report a comprehensive study of both diffusion and structure of these two tracer species in an environment crowded by quenched configurations of polymers at increasing density. We analyze in detail how the tracer-polymer affinity and the system density affect transport as compared to the emergence of specific static spatial correlations. In particular, we find that, while hardly any differences emerge in the diffusion properties of WCA and CS particles, the propensity to develop structural order for large crowding is strongly frustrated for CS particles. Surprisingly, for large enough affinity for the crowding matrix, the diffusion coefficient of WCA tracers display a nonmonotonic trend as their density is increased when compared to the zero affinity scenario. This waterlike anomaly turns out to be even larger than what observed for CS particle and appears to be rooted in a similar competition between excluded-volume and affinity effects.

DOI: [10.1103/PhysRevE.102.032618](https://doi.org/10.1103/PhysRevE.102.032618)**I. INTRODUCTION**

Diffusion process are well described by conventional fluid mechanics for dilute mixtures in noncomplex geometries. This is not the case in biological environments, such as the cell, which contains a high diversity of macromolecular species at high concentrations in strongly confining geometries. For instance, in a cell macromolecules such as proteins, polysaccharides, nucleic acids and other smaller molecules occupy volume fractions typically larger than 30% of the available space [1–5].

While excluded-volume effects in such contexts are often referred to as *macromolecular crowding* [6], other factors strongly affect diffusion-based processes in biological media, most importantly many nonspecific interactions, such as van

der Waals, electrostatic and hydrodynamic interactions [7]. Indeed, crowded environments may influence the behavior of biomolecules in many subtle ways. For example, it has been proved that stabilization or destabilization of proteins and protein complexes may be observed, depending on the relative strength of weak nonspecific enthalpic interactions and purely entropic excluded-volume interactions [8].

Overall, the influence of crowding and nonspecific interactions on single-particle diffusion are not fully understood [6]. While single-particle tracking (SPT) experiments and fluorescence correlation spectroscopy (FCS) allow one in principle to measure the diffusion coefficient of fluorescently tagged tracers *in vivo* [9], the interpretation of the results in the context of simple models is still a difficult task [7]. One of the easiest and most interesting workarounds to this problem is to measure diffusion in controlled artificial environments, created so as to mimic only selected specific features of the overwhelming cellular complexity. For example, tunable crowded environments where nonspecific interactions are virtually silenced have been realized using highly concentrated polymer solutions, such as dextran or ficoll [10,11], where diffusion has

<sup>\*</sup>thiagoponogueira@gmail.com<sup>†</sup>hfrota@ufam.edu.br<sup>‡</sup>Francesco.Piazza@cnrs-orleans.fr<sup>§</sup>jrbordin@ufpel.edu.br

been investigated, e.g., through FCS [10] and fluorescence recovery after photobleaching (FRAP) spectroscopy [11].

In addition to the above mentioned and other experimental studies, numerical simulations have proved invaluable to dissect the subtle influence of the environment on the mobility of tracers [7]. Many different computational techniques have been employed to this end, from Monte Carlo simulations [12,13] and Brownian dynamics (BD) [14–20] to molecular dynamics simulation [18,21–23].

As a general rule, biological macromolecules tend to have variably flexible structures. Therefore, when two macromolecules approach each other, their branches can become entangled and nonspecific attractive and/or repulsive interactions may come into play. This effect is expected to influence to a substantial extent macromolecular diffusion in crowded media. This, in turn, implies that models based exclusively on hard spheres may miss important features of the tracer-environment interactions [24].

In the simplest approximation beyond hard-core interactions, core-softened colloids and proteins may be characterized by the presence of two length scales, a short-range attraction and a long-range repulsion [25,26]. The repulsion can be caused by a soft shell, as in the case of polymeric brushes [27–33] and star-polymers [34–37], or by electrostatic repulsion in charged colloids, macromolecules, lysozyme and spherical proteins [12,26,38,39], while the attraction is caused by van der Waals forces or solvent effects [40,41].

Core-softened potentials have also been largely employed to study systems with water-like anomalies [12,42–44] along with the related confinement effects [45–47]. In fact, for most materials the diffusion coefficient decreases when the pressure (or density) increases. However, anomalous materials such as water [48], silicon [49], and silica [50] also display a diffusion anomaly, characterized by a maximum in the diffusion coefficient at constant temperature. Therefore, a relevant question that arises is how crowded media may influence the diffusion of core-softened tracer particles immersed in a polymeric environment with respect to hard-core particles. To answer this question, in this paper we employ large-scale Langevin dynamics simulations and characterize how excluded-volume effects and tracer-crowder interactions affect tracer diffusion. More precisely, we consider two species of tracers, (i) hard-core spherical particles modeled by the well known Weeks-Chandler-Andersen (WCA) purely repulsive potential [51], and (ii) core-softened particles, displaying a dual-length scale hard core–soft corona structure. To mimic macromolecular crowding, we inject these tracer molecules in a complex static polymeric solution realized via a coarse-grained model [52]. Our main goal is to investigate single-particle diffusion and static space correlation of these two molecular species immersed in the polymer matrix. More precisely, we aim at analyzing how the tracer-polymer affinity and the polymer density affect the transport and spatial correlations of the tracer particles.

## II. MODEL AND SIMULATION DETAILS

A fluid of tracer molecules with packing fraction  $\phi_f$  is immersed in a static polymer matrix such as the one shown in Fig. 1. We consider two types of tracer-tracer interactions.

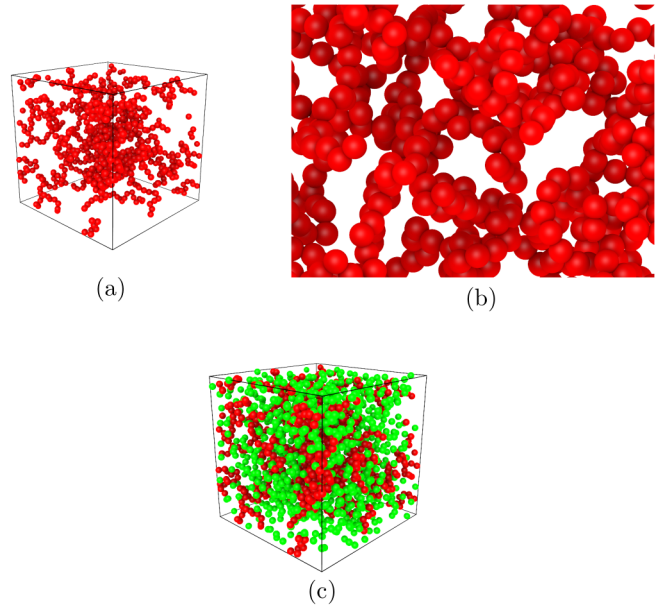


FIG. 1. Illustration of the three-dimensional tracer-polymer system analyzed in our simulations. (a) System snapshot with only polymers obstacles at volume occupancy  $\phi_p = 0.05$ . (b) Zoomed snapshot with only polymers obstacles at the same volume fraction as seen in (a), where a complex structure of voids can be appreciated. (c) Snapshot of the whole system, comprising the polymer obstacles (red) and the tracer particles (green).

Single-length repulsive tracers interact through the WCA potential,  $U_{\text{WCA}}$ , namely,

$$U_{\text{WCA}}(r) = \begin{cases} 4\epsilon \left[ \left( \frac{\sigma}{r} \right)^{12} - \left( \frac{\sigma}{r} \right)^6 + \frac{1}{4} \right], & r \leq r_c, \\ 0, & r \geq r_c. \end{cases} \quad (1)$$

The WCA potential is a standard potential energy function in soft matter, which was originally proposed to model a soft-core, purely repulsive potential [51]. It is obtained by cutting a standard 12-6 LJ potential at the position of the minimum,  $r_c = 2^{1/6}\sigma$ , and shifting this function upwards by an energy equal to the well depth. As a consequence, the potential is zero above  $r_c$  and has a sharp increase to  $+\infty$  below  $r_c$ . The resulting potential is the soft-core purely repulsive red curve in Fig. 2.

Two-length scales repulsive tracers interact through a core-softened interaction  $U_{\text{CS}}$ ,

$$U_{\text{CS}}(r) = 4\epsilon \left[ \left( \frac{\sigma}{r} \right)^{12} - \left( \frac{\sigma}{r} \right)^6 \right] + u_0 \exp \left[ -\frac{1}{c_0^2} \left( \frac{r - r_0}{\sigma} \right)^2 \right]. \quad (2)$$

The potential Eq. (2) consists of the sum of a short-range Lennard-Jones term and a long-range Gaussian function centered at  $r_0$ , with depth  $u_0$  and width  $c_0$ . The potential Eq. (2) can be parameterized to have distinct shapes [41,42]. Here we use the parameters  $u_0 = 5\epsilon$ ,  $c_0^2 = 2.0$ , and  $r_0/\sigma = 0.7$ , which lead to the repulsive ramp depicted by the blue curve in Fig. 2. This shape was extensively applied to study systems with

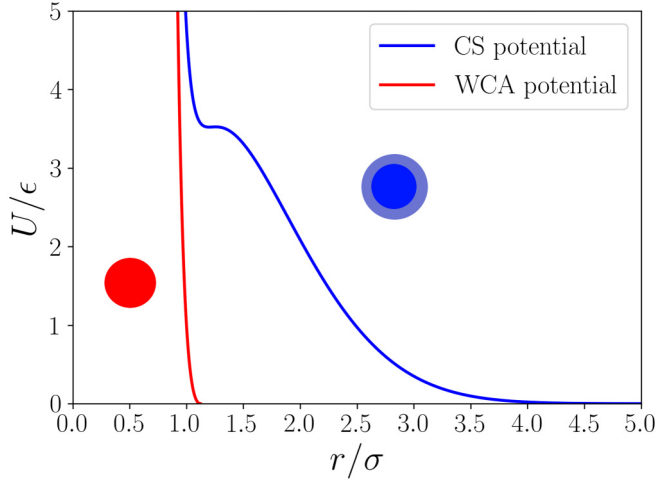


FIG. 2. Weeks-Chandler-Andersen (WCA) and core-softened (CS) interaction potentials between two tracer particles. Inset: schematic depiction of the particles, in red the WCA particle with its core (first length scale at  $r = 1.2\sigma$ ), in blue the CS particle with its core (first length scale at  $r = 1.2\sigma$ ) and the soft corona (second length scale at  $r = 2.0\sigma$ ).

water-like anomalies [42–44], in view of its two characteristic length scales. The first one is  $r_1 = 1.2\sigma$ , where the force has a local minimum, while the longer length scale is  $r_2 = 2\sigma$ , where the fraction of imaginary modes of the instantaneous normal modes spectrum has a local minimum [53]. The cutoff radius for this interaction was fixed as  $r_c^{CS} = 3.5\sigma$ .

Five different polymer matrices were generated for each point in parameter space by extracting independent configurations from  $NVT$  equilibrium molecular dynamics of  $N_c$  polymer chains consisting of an equal number  $N_m$  of monomers of the same size  $\sigma$  each, interacting along the polymer backbone through a standard finitely extensible nonlinear elastic (FENE) potential [52,54],

$$U_{\text{FENE}}(r) = \begin{cases} -\frac{1}{2}kR_0^2 \ln \left[ 1 - \left( \frac{r}{R_0} \right)^2 \right], & r \leq R_0, \\ \infty, & r \geq R_0. \end{cases} \quad (3)$$

Here  $k$  is the elastic constant and  $R_0$  is the limit distance for bond elongation. In this work we used the same parameters as in Ref. [52], namely,  $k = 30\epsilon/\sigma^2$  and  $R_0 = 1.5\sigma$ . Self-avoidance of the polymer chains was enforced by means of a Weeks-Chandler-Andersen (WCA) potential, acting for simplicity among all monomer pairs. Once the required number of independent polymer matrices were generated, these were frozen and the fluid tracer molecules were injected in the simulation box and the production runs started, the tracers being the only mobile species in all the simulations.

The interaction between tracers and the polymer matrix was modeled as a standard LJ interaction

$$U_{\text{LJ}}(r) = \begin{cases} 4\epsilon_{\text{AB}} \left[ \left( \frac{\sigma}{r} \right)^{12} - \left( \frac{\sigma}{r} \right)^6 \right], & r \leq r_c \\ 0, & r \geq r_c, \end{cases} \quad (4)$$

with cutoff  $r_c^{LJ} = 2.5\sigma$ . The tracer-polymer affinity  $\epsilon_{\text{AB}}$  (A for polymer and B for tracers) is one of the main pa-

rameters whose effect on the tracer diffusion we want to investigate, with the aim of clarifying the competition between tracer-tracer and tracer polymer interactions.

All the simulations (generation of the polymer configurations and production runs) were carried out in the  $NVT$  ensemble, enforced by means of Langevin dynamics (LD) [55] in reduced LJ units, namely,

$$r^* \equiv \frac{r}{\sigma}, \quad \rho^* \equiv \rho\sigma^3, \quad t^* \equiv t \left( \frac{\epsilon}{m\sigma^2} \right)^{1/2}, \quad T^* \equiv \frac{k_B T}{\epsilon}, \quad (5)$$

where  $m$  is the mass of tracers and monomers. The temperature was kept constant via the Langevin thermostat at  $T^* = 4.45$ , which ensured that the system was fluid even at high densities for both tracer species. The packing fraction is defined as  $\phi = Nv/L^3$ , where  $L$  is the side of the (cubic) simulation box,  $v = \pi\sigma^3/6$  is the single-particle volume, and  $N = N_t + N_m N_c$  is the total number of particles, comprising  $N_t$  tracers and  $N_m N_c$  monomers belonging to the ensemble of polymer chains. In practice, we fixed  $N_c = 100$  and  $N_m = 40$  in all simulations and varied  $L$  and  $N_m$  to fix the fluid and polymer packing fractions,  $\phi_f$  and  $\phi_p$ , at the chosen values. In the first set of simulations, we fixed the fluid packing fraction  $\phi_f = 0.1$  and varied the polymer packing fraction  $\phi_p$  from 0.001 up to 0.1. In a second set of simulations, we kept the polymer volume fraction fixed instead at  $\phi_p = 0.1$  and varied  $\phi_f$  from 0.1 up to 0.4 with the aim of investigating the effects of self-crowding. The time step used in the simulations was  $\delta t = 0.001$  (reduced units), and periodic boundary conditions were enforced in the three Cartesian directions. Each simulation comprised a first relaxation and equilibration run ( $10^6$  steps) followed by  $10^7$  steps for the production runs. To ensure that the system had reached equilibrium, the kinetic and potential energy were monitored as functions of time. All simulations were carried out using the LAMMPS simulation package [56].

Five independent simulations were performed at each point in parameter space, starting from as many independent random configurations of tracers and polymers. The diffusion coefficient was computed by fitting the long-time linear trend of the mean-square displacement (MSD) as function of time, namely,

$$D = \lim_{t \rightarrow \infty} \frac{\mu_2(t)}{6t}, \quad (6)$$

where the MSD  $\mu_2(t) = \langle \langle [\vec{r}(t+t_0) - \vec{r}(t_0)]^2 \rangle \rangle$  at a given lag  $t$  was computed by the usual double average over the five independent runs and different time origins  $t_0$ . The fluid structure was analyzed by computing the radial distribution function (RDF)  $g(r)$ . More precisely, we evaluated the RDF between particle A (polymer) and B (tracer)  $g_{\text{AB}}(r)$  and the tracer-tracer RDF,  $g_{\text{BB}}(r)$ .

We point out that in this work hydrodynamic interactions (HI) are neglected, as the fluid is treated implicitly through the simple Langevin scheme. Indeed, HI have been shown to be important in accounting for the observed reduction of translational diffusion coefficient in very crowded, heterogeneous cell-like systems, i.e., for densities around 300 mg/ml [57]. However, HI effects are expected to be prominent for nonspherical systems and in the presence of a wide range of molecular sizes in the system. In particular, one may expect

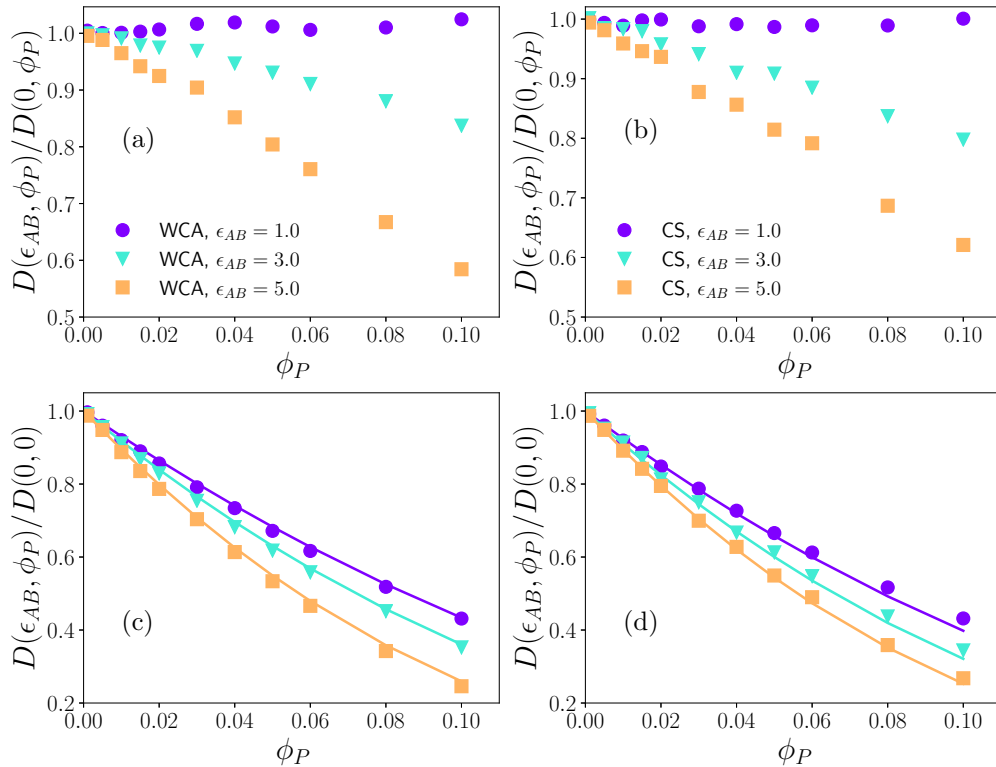


FIG. 3. Diffusion coefficient of tracer molecules,  $D(\epsilon_{AB}, \phi_P)$ , as a function of the polymer volume fraction  $\phi_P$  for different values of the tracer-polymer affinity,  $\epsilon_{AB}$ . Left: WCA tracers. Right: CS tracers. Upper panels. The diffusion coefficients are normalized to the  $\epsilon_{AB} = 0$  value at the same values of  $\phi_P$  to highlight the effect of the tracer-polymer affinity. Lower panels. The diffusion coefficients are normalized to the value at  $\epsilon_{AB} = 0, \phi_P = 0$ , to make the effect of varying both parameters explicit. Solid lines correspond to one-parameter fits to a model of diffusion in porous media, where the polymer matrix is modeled as an effective quenched suspension of hard spheres, see Eq. 7. Points are the averages obtained from five independent runs. Error bars are smaller than the size of symbols.

that inclusion of HI would become important when the focus is on how crowding and molecular size shapes diffusion for strongly nonspherical, heterogeneous systems. In the case of the present study, we concentrate on rather homogenous spherical systems at moderate crowding ( $\phi_P \leq 0.1$ ), where the radius of tracers is not varied. Therefore, we expect that HI should not introduce a substantial bias in the *normalized* diffusion coefficients, the main observable investigated in this work.

As a final remark, we note that in the following all physical quantities are expressed in reduced LJ units, while we will omit the superscript \* for the sake of clarity.

### III. RESULTS AND DISCUSSION

The first set of simulations refers to a fluid of tracers whose volume fraction was fixed at  $\phi_f = 0.1$  and immersed in a polymer matrix that occupies increasing fractions of the available volume. In the second set of simulations, we varied the packing fraction of the tracers while keeping the crowding polymer matrix at  $\phi_P = 0.1$ . In both cases, we considered both kinds of tracer-tracer interactions, namely, single-length scale (WCA) and double-length scale (CS), and progressively increased the strength of the tracer-polymer interaction,  $\epsilon_{AB}$ , from zero.

#### A. Diffusion and structure of the tracer fluid at different polymer packing fractions $\phi_P$

The results of our simulations are illustrated in Fig. 3, where we chose two different ways to normalize the data. The effect of the tracer-polymer affinity  $\epsilon_{AB}$  is best singled out by normalizing the measured diffusion coefficient through  $D(0, \phi_P)$ . Each point in the plot then quantifies the reduction in mobility caused by the tracer-crowder attractive interaction irrespective of the additional reduction due to crowding, i.e., excluded-volume. The first observation is that, surprisingly, a moderate attractive interaction seems to have no effect on the tracer mobility (circles in the upper panels). Increasing the strength of the tracer-polymer interaction beyond the value  $\epsilon_{AB} = \epsilon$ , that is, the typical repulsive energy at the monomer-tracer contact distance, tracer mobility appears progressively more and more hindered. In other words, a crowded environment that is also somewhat *sticky* causes more hindrance to tracer diffusion. This effect is larger the more crowded the environment, with  $D(\epsilon, \phi_P)/D(\epsilon = 0, \phi_P)$  appearing to decrease linearly with the crowding packing fraction  $\phi_P$ . It is interesting to note that, based on the findings reported in Ref. [58], we might expect the slope of the straight lines  $D(\epsilon_{AB}, \phi_P)/D(0, \phi_P)$  to depend nonmonotonically on the tracer-polymer interaction strength  $\epsilon_{AB}$ . However, to investigate whether the interesting nonmonotonicity reported for the setting considered in Ref. [58] would also show up in our



system would require exploring more finely spaced values of  $\epsilon_{AB}$ , possibly in the predicted interval  $\epsilon_{AB} \in [1, 3] k_B T$ .

The second observation is that the presence of multiple length scales in the tracer-tracer interaction does not seem to induce noticeable differences in the way their mobility is shaped by the interaction with the environment. As a matter of fact, the reduction in diffusion for the WCA and CS fluid particles are very similar. While this may come to little surprise, as the tracer volume fraction is still on the low side ( $\phi_f = 0.1$ ), we shall see that this observation on mobility is not mirrored by the corresponding static structure of the tracer fluid, which is characterized by different spatial correlations induced by the crowders that indeed appear to depend on the kind of tracer-tracer interaction.

The lower panels in Fig. 3 show the same data normalized in a different fashion, intended to highlight the combined action of crowder-tracer affinity and crowding volume fraction on diffusion. It can be clearly appreciated that an environment that is both crowded and somewhat *sticky* induces a substantial slowing down of the mobility. Tracers appear to loose between 60 and 70% of their mobility at a polymer packing fraction as low as 10% when the tracer-polymer attractive energy is between 3 and 5 times the typical energy  $\epsilon$ . Again, this normalization does not reveal substantial differences in mobility ascribed to the kind of tracer-tracer interaction in the bulk.

It is instructive to compare our results with known predictions of diffusion in complex porous media. In such context, the ratio of the tracer diffusivity in the matrix to the Stokes-Einstein diffusivity  $D_0$  in the pure suspending fluid is known as the so-called *tortuosity*  $\tau$ . For a static matrix of spherical particles of diameter  $\sigma_1$  with volume fraction  $\phi$ , one has [59]

$$\frac{D(\phi)}{D_0} \equiv \tau(\phi) = (1 - \phi)^\nu [1 - \lambda_p(\phi)]^{a+b\lambda_p(\phi)}, \quad (7)$$

where  $\nu = 0.4$ ,  $a = 4.2$ ,  $b = 0.55$ , and  $\lambda_p(\phi)$  is the ratio of tracer particle diameter  $\sigma$  to the typical pore diameter  $\sigma_p(\phi)$ ,

$$\lambda_p(\phi) \equiv \frac{\sigma}{\sigma_p(\phi)} = \left(\frac{\sigma}{\sigma_1}\right) \frac{3\phi}{1 - \phi}. \quad (8)$$

It is interesting to inquire whether our polymer matrices behave effectively as simple quenched suspensions of hard spheres by treating the diameter of such effective spheres  $\sigma_1$  as an adjustable parameter. The fits shown in the bottom panels in Fig. 3 reveal that our polymer matrices indeed behave as quenched suspensions of hard spheres over the whole range of parameters considered. More precisely, as the tracer-polymer interaction strength increases, the typical effective pore size decreases, showing that *stickier* polymer matrices slow down tracers as quenched suspensions with smaller pores would do. This analogy also allows us to compute the equivalent void percolation threshold of the polymer matrix  $\phi_p^c$ , that is, the critical packing fraction where the pore size equals the tracer size. From the condition  $\lambda_p = 1$ , Eq. (8) gives immediately

$$\phi_p^c = \frac{\sigma_1}{3\sigma + \sigma_1}. \quad (9)$$

The best-fit values of the size of the effective crowding spheres and the corresponding percolation thresholds are reported in Table I.

TABLE I. Best-fit values of the diameter of the effective crowding hard spheres,  $\sigma_1$ , obtained by fitting Eq. (7) to our data over the whole range of polymer packing fraction  $\phi_p$ . The corresponding void percolation thresholds  $\phi_p^c$  computed from Eq. (9) are also reported.

$\epsilon_{AB}$	WCA		CS	
	$\sigma_1/\sigma$	$\phi_p^c$	$\sigma_1/\sigma$	$\phi_p^c$
0.0	$1.85 \pm 0.02$	$0.381 \pm 0.004$	$1.89 \pm 0.02$	$0.386 \pm 0.002$
1.0	$1.91 \pm 0.02$	$0.389 \pm 0.002$	$1.86 \pm 0.03$	$0.383 \pm 0.004$
3.0	$1.57 \pm 0.01$	$0.343 \pm 0.001$	$1.51 \pm 0.02$	$0.335 \pm 0.003$
5.0	$1.21 \pm 0.01$	$0.287 \pm 0.002$	$1.26 \pm 0.01$	$0.296 \pm 0.002$

The similar trends observed in the mobility of WCA and CS particles might still conceal some more conspicuous difference in the structural reorganization of the tracer fluid induced by the sticky crowding matrices. To investigate this aspect, it is instructive to compute the radial distribution function (RDF), both for tracer-tracer pairs (BB) as well as for tracer-monomer pairs (AB). Figure 4 illustrates the behavior of the polymer-fluid RDF,  $g_{AB}(r)$ . Both kind of fluids appear to develop an increasing degree of structural organization in the vicinity of the polymer matrix as the polymer-tracer affinity increases beyond  $\epsilon_{AB} = 1$ . However, this analysis reveals that CS particles are much less prone to affinity-induced structural organization around the crowders. This observation can be interpreted as a direct result of the competition between different length scales in the repulsion between CS particles, which appears to induce some frustration in the spatial ordering of such tracers in the presence of crowding.

A direct inspection of the tracer-tracer RDFs  $g_{BB}(r)$  (Fig. 5) confirms that structural ordering is globally more hindered in the CS fluid. Interestingly, WCA particles get more and more structured around each other at large values of  $\epsilon_{AB}$  and the first and second coordination shells appear to become populated at essentially the same rate [see Fig. 5(d)]. This is most likely a *templating* effect, whereby the chain connectivity of the sticky polymer matrix causes ordered association of the tracers along the polymer chains, thus promoting the development of structural correlations in the vicinity of the crowders. This effect would most likely disappear in the case of crowding agents whose microstructure would be incommensurate to that of the tracers. We will come back to this effect in the next section. By contrast, the dual length-scale repulsion of CS particles appears to essentially suppress any appreciable structuring in the first coordination shell, while the second shell becomes more and more populated, even if to a much lesser extent when compared to WCA particles [see arrow in Fig. 5(h)].

## B. The effect of self-crowding on diffusion

It is interesting to reverse the diffusion analysis illustrated above, where the fluid packing fraction was held fixed at  $\phi_f = 0.1$ , while we investigated the combined effect of  $\epsilon_{AB}$  and the crowding volume occupancy,  $\phi_p$ . In this section, we analyze the results of simulations where the crowding density was fixed at the same moderate value, i.e.,  $\phi_p = 0.1$ , while we

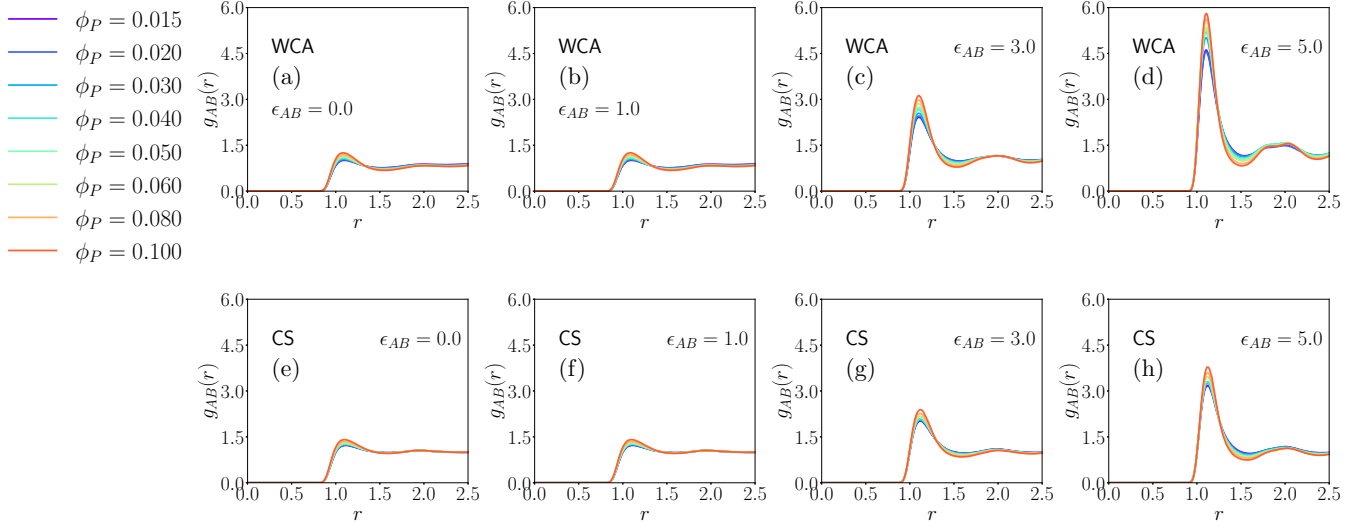


FIG. 4. The polymer-tracer RDF  $g_{AB}(r)$  for WCA (top) and (CS) particles for different values of the tracer-polymer affinity.

increased progressively self-crowding by letting  $\phi_f$  and  $\epsilon_{AB}$  vary. To isolate the effect of the polymer-tracer affinity, we plot in Fig. 6 the diffusion coefficient of tracers  $D(\epsilon_{AB}, \phi_f)$  normalized to the purely repulsive value at the same density,  $D(0, \phi_f)$ . As a first observation, it can be clearly appreciated that varying the fluid packing fraction (self-crowding) seems to have a less dramatic effect on diffusion than varying the crowding density. For low affinity,  $\epsilon_{AB} = 1.0$ , WCA and the CS tracers display an approximately constant diffusion coefficient, mirroring the corresponding trend observed in the reversed situation (see Fig. 3, top panels).

An interesting phenomenon is observed in the high-affinity case. When  $\epsilon_{AB} = 5.0$ , both tracer species display a waterlike diffusion anomaly, more pronounced in the case of WCA tracers. It is clear from figure 6 that the diffusion constant increases as  $\phi_f$  increase, reaches a maximum at  $\phi_f \cong 0.2$

and then decreases again as the fluid density increases further. While for CS molecules this anomalous behavior is well known and directly ascribed to the dual-length repulsion [42,44], it appears rather unexpected in the simple repulsive WCA fluid.

Some insight into this unexpected result can again be gathered by looking at the radial distribution functions at increasing values of  $\phi_f$  in the high-affinity case for WCA tracers (Fig. 7). More precisely, one notices that the effect of increasing the fluid density is to progressively lower the fraction of tracers adsorbed on the polymer matrix. This behavior is clearly illustrated by the decrease of both the first and second peaks in the polymer-tracer RDF,  $g_{AB}(r)$  [Fig. 7(a)]. At the same time, while the polymer-tracer interface becomes less organized, the tracers start developing more short-range order. This is reflected by the increase of the first peak of

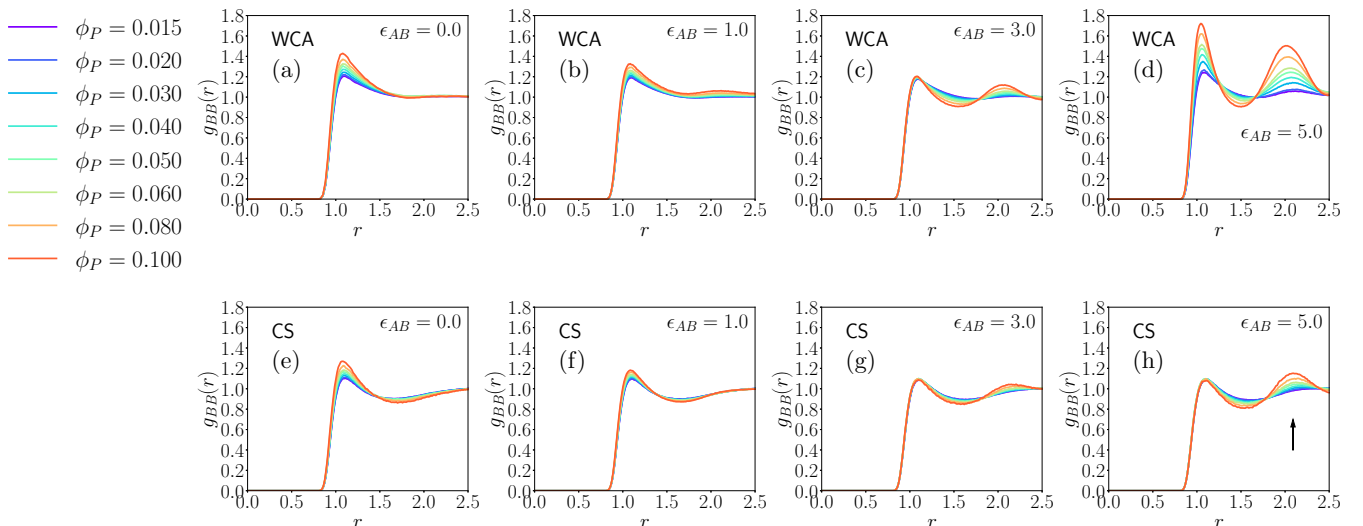


FIG. 5. The tracer-tracer RDF  $g_{BB}(r)$  for WCA (top) and (CS) particles for different values of the tracer-polymer affinity.

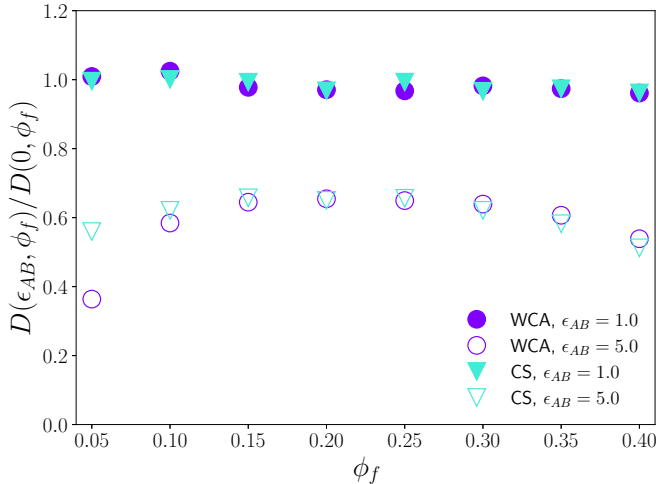


FIG. 6. Diffusion coefficient of tracers normalized to the purely repulsive values  $D(0, \phi_f)$  as a function of the fluid volume fraction  $\phi_f$  for two values of  $\epsilon_{AB}$ .

the tracer-tracer RDF,  $g_{BB}(r)$  [Fig. 7(b)]. To confirm this, we divided the tracers in two classes: adsorbed and bulk tracers. To this end, 1000 system snapshots were analyzed based on the inter-tracer-polymer bonding, in a similar manner as done in previous works to characterize colloids aggregates [41,60,61]. Tracers were considered adsorbed when they lie at distances smaller than  $1.25\sigma$  from one polymer monomer. If the distance was larger than this threshold, the tracer was considered in the bulk.

The adsorbed and bulk tracer-tracer RDFs are shown in Figs. 7(c) and 7(d), respectively. It can be appreciated that the increase in the first peak of the total tracer-tracer RDF, Fig. 7(b), comes from the contribution of bulk tracers, Fig. 7(d)—both grow as the density increases. At the same time, this analysis provides a visual and quantitative rationalization of the aforementioned *templating* effect, which manifests itself in increased tracer-tracer organization at the interface at large values of  $\epsilon_{AB}$ .

It can be appreciated that such effective attractive tracer-tracer interaction appears to be rather long-range, extending over about 4 tracer diameters. This effect can be observed in Fig. 7(c): the peaks decay as  $\phi_f$  increases. Furthermore, we see here clearly that self-crowding has a disruptive effect on the templating action exerted by the polymer matrix on tracers, increasingly promoting structural order of the tracer fluid in the bulk [see again Fig. 7(d)].

To further clarify how the polymer *stickiness* modulates the effect of self-crowding, we evaluated the MSD of adsorbed and bulk tracers (Fig. 8). In the case of low affinity, there appears to be no apparent difference between adsorbed and bulk tracers – both species diffuse similarly regardless of the fluid density [Figs. 8(a), 8(b) and 8(c)]. However, at higher affinity, it is clear that at low tracer densities the adsorbed tracers display a reduced mobility with respect to bulk tracers [Fig. 8(d)]. Increasing self-crowding, the two species recover the same mobility, starting at a value around  $\phi_f = 0.20$ —the point where the tracer diffusion coefficient has a maximum

(see again Fig. 6). The different evolution of the weight associated with bulk and adsorbed tracers with the overall tracer density is presumably the reason behind the nonmonotonic trend observed in Fig. 6. In other words, as we increase the fluid density, less and less tracers are adsorbed by the polymer matrix, thereby raising the number of unconstrained, fully mobile molecules in the bulk. However, increasing the fluid density further, the self-crowding effects become more prominent and the mobility of bulk tracers starts decreasing as the fluid becomes more and more structured (see also the black arrows in Fig. 7). Therefore, the combination of highly sticky obstacles and high tracers density can lead to unexpected dynamical behaviors.

#### IV. CONCLUSIONS

In this paper, we employed large-scale Langevin dynamics simulations to investigate the mobility of tracer particles diffusing in a static matrix consisting of quenched polymer chains of equal-sized monomers. The two main parameters varied were the volume fraction occupied by the polymer matrix and the strength of a short-range, nonspecific attractive interaction causing tracer particles to spend longer time in the vicinity of the crowders. Furthermore, we focused on two types of tracer particles, characterized by different tracer-tracer repulsive interactions. In particular, we considered core-softened tracers (CS), characterized by a dual-length repulsive potential as compared to purely repulsive, shifted Lennard-Jones particles (WCA).

We found that excluded-volume interactions, i.e., crowding, reduce the tracer diffusion coefficient, all the more so the larger the polymer-tracer affinity. At the moderate tracer volume fraction considered in this paper ( $\phi_f = 0.1$ ), we found no appreciable signature of the kind of tracer-tracer interactions in the measured diffusivity. The mobility of CS and WCA particles decreased with increasing crowding and increasing affinity following practically indistinguishable trends. In particular, we found that, for all the values of the attractive energy strength considered, the *sticky* crowding matrices behaved as porous media consisting of effective quenched suspensions of purely repulsive hard spheres, as gauged by fitting a tortuosity model to our data.

If the measured diffusion coefficients bore no blueprint of the underlying tracer-tracer interactions, the same was not true for static spatial correlations. In particular, for large crowding tracer affinity, the core-softened tracers showed a considerably lower propensity to structure around the polymers, whereas WCA particles showed substantial short- and intermediate-range order, increasing with the volume fraction of crowders.

To explore further the distinctive signature of the tracer-tracer repulsion in the high affinity case, we ran a series of simulations at increasing density of tracers and intermediate crowding ( $\phi_p = 0.1$ ) for  $\epsilon_{AB} = 5$ , comparing the measured diffusion coefficient to the zero affinity case. While we recovered the known water-like anomaly for CS particles, i.e., a nonmonotonic trend of the diffusion coefficient as a function of the tracer density for high affinity, we found an even more pronounced anomaly of the same kind for the WCA particles.

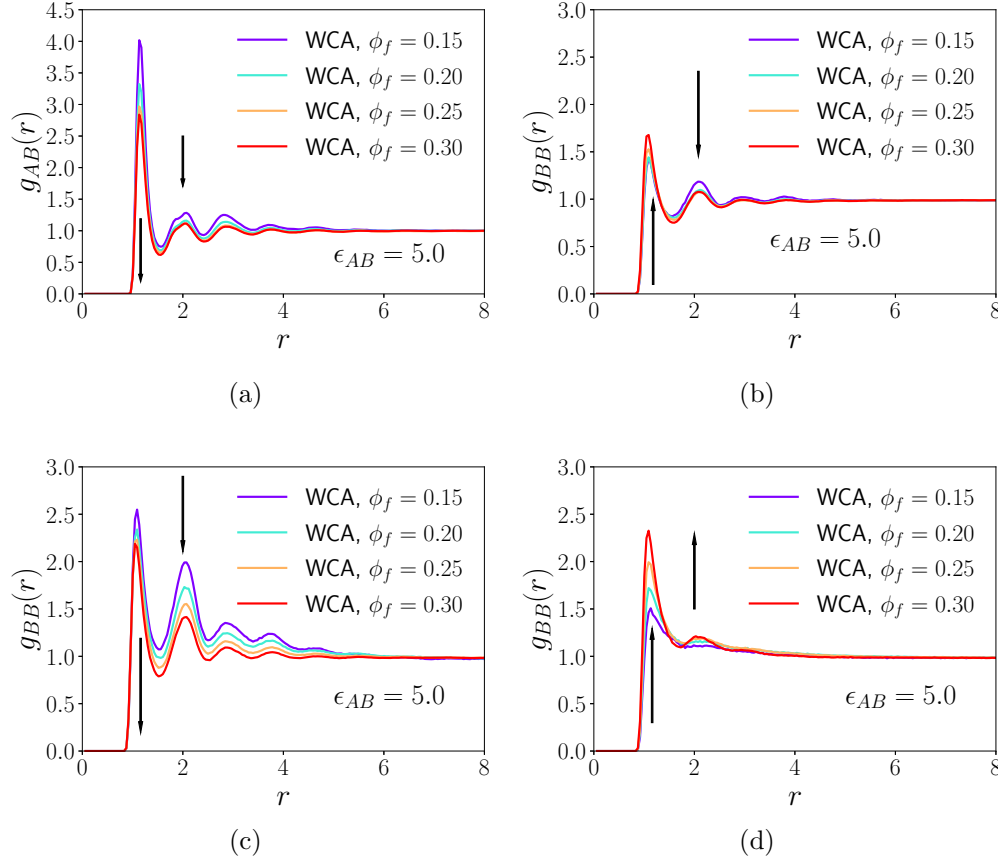


FIG. 7. Total (adsorbed + bulk) polymer-tracer (a) and tracer-tracer (b) radial distribution functions at increasing values of the tracer packing fraction. Bottom panels: the tracer-tracer RDF for adsorbed tracers (c) and bulk tracers (d). The polymer matrix packing fraction is  $\phi_P = 0.1$ .

This kind of anomaly, which does not seem to be directly ascribed to dual-length repulsion, is more deeply, and likely more generally rooted in the competition between the confinement and the attraction exerted on tracers by the polymeric network. For dilute tracer fluids, an increase in self-crowding is seen to induce a progressive desorption of tracers from the polymer matrix, while the fluid gets more and more structured in the bulk. The apparent result of this is that a little increase in  $\phi_f$  from the very dilute case reduces  $D(\epsilon_{AB} = 5, \phi_f)$  less than what observed in the zero-affinity case, i.e., less than  $D(\epsilon_{AB} = 0, \phi_f)$ . It is worth recalling that a relatively ample body of literature exists reporting a nonmonotonic trend of the diffusion coefficient in the presence of crowding and tracer-crowder attractive interactions as the strength of the latter is increased. This scenario, also rooted in the competition between confinement and attraction, appears rather general, from quenched-annealed mixtures of hard spheres [58], to ions in a charged polymer gel [62], nanoparticles in polymer melts [63], and simple hard-sphere-like colloids [64]. However, despite the large body of work in this area, further work seems to be needed to gather a more comprehensive picture of tracer diffusion in the presence of crowded and attractive media in the regime where self-crowding effects become important.

As a final remark, we point out that no evidence of anomalous diffusion was ever found in the results of our

simulations. In this kind of systems, one could expect to observe (at least) two kinds of anomalous diffusion in some regimes, (i) transient anomalous behavior as a crossover between short-time diffusion and long-time diffusion and (ii) (possibly asymptotic) anomalous diffusion of the single-file kind near the void percolation threshold. The former case would flag the presence of some caging effect, whereby a quick diffusive exploration of the local cage is followed by a much slower diffusion over the large-scale ensemble of cages. We did not find any evidence of a transition between short-time and long-time diffusion for any of the parameter choices considered in this work. The reason is likely to be related to the specific way the space where tracers diffuse is crowded with obstacles. Since these are self-avoiding polymer chains, the presence of cages at moderate packing fraction (we considered up to  $\phi_P = 0.1$ ) should be negligible. It would be interesting to investigate how tracers diffuse within much denser crowding matrices to explore whether caging effects emerge at all in the presence of connected crowders. Regime (ii) is a subtler matter altogether. While some evidence of anomalous diffusion has been reported in the case of quenched-annealed mixtures of hard spheres [65,66], it is uncertain whether this would be a general feature of obstructed diffusion. In the present work, we did not explore the regime close to the void percolation threshold, neither we performed quantitative characterizations of the



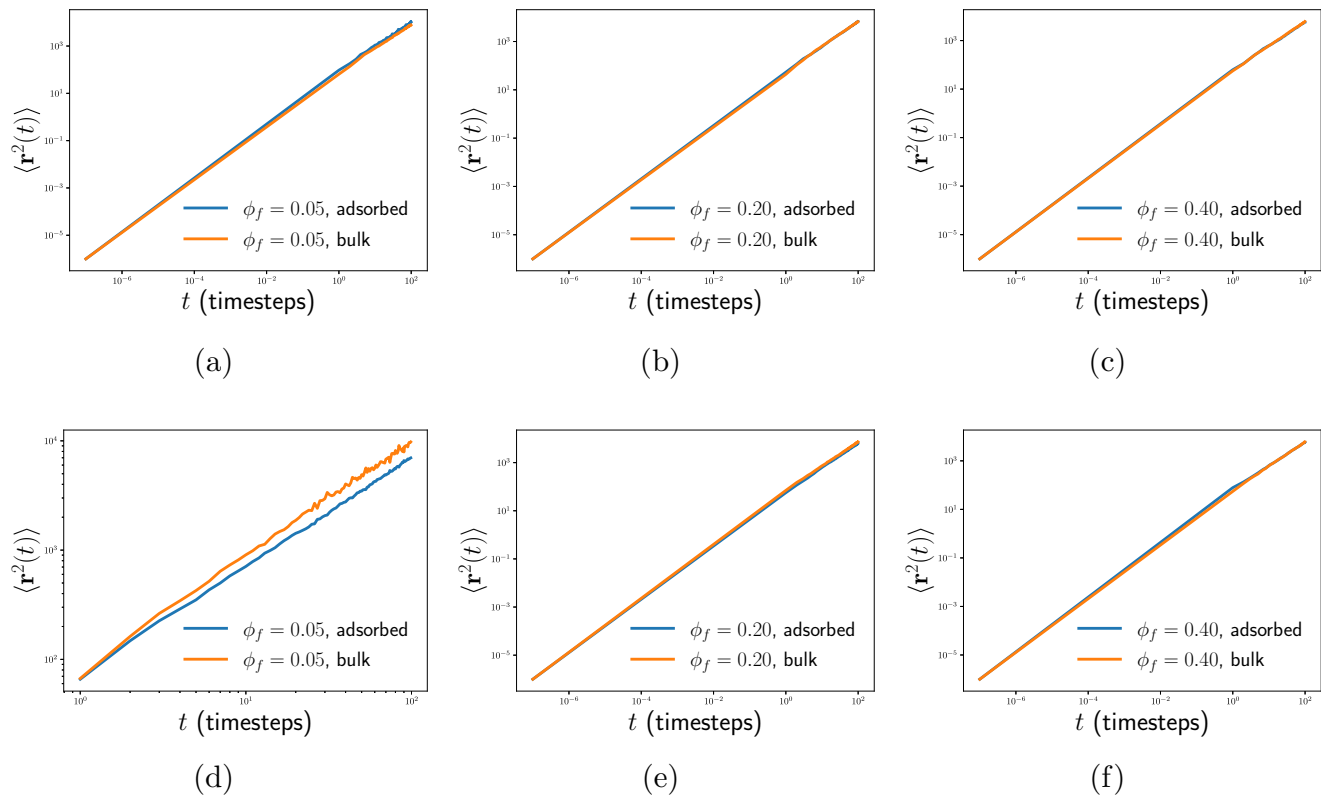


FIG. 8. MSD for adsorbed and bulk tracers. The top panels illustrate the low-affinity case, while the bottom ones depict the high-affinity case. The fluid densities are: 0.05 (a, d); 0.20 (b, e); 0.40 (c, f). The polymer matrix packing fraction is  $\phi_p = 0.1$ .

void size distributions. It would be extremely interesting to couple these kinds of studies to measurements of tracer mobility, to investigate whether anomalous diffusion related to a phase transition of the void percolation type emerges in the presence of connected obstacles such as immobile polymer chains.

#### ACKNOWLEDGMENTS

This study was financed in part by the Coordenação de Aperfeiçoamento de Pessoal de Nível Superior (CAPES), Finance Code 001. J.R.B. acknowledge the Brazilian agencies CNPq and FAPERGS for financial support. F.P. is greatly indebted to Giuseppe Foffi for illuminating discussions.

- [1] S. B. Zimmerman and S. O. Trach, Estimation of macromolecule concentrations and excluded volume effects for the cytoplasm of escherichia coli, *J. Mol. Biol.* **222**, 599 (1991).
- [2] S. B. Zimmerman and A. P. Minton, Macromolecular crowding: Biochemical, biophysical, and physiological consequences, *Annu. Rev. Biophys. Biomol. Struct.* **22**, 27 (1993).
- [3] H.-X. Zhou, Protein folding and binding in confined spaces and in crowded solutions, *J. Mol. Recogn.* **17**, 368 (2004).
- [4] H.-X. Zhou, G. Rivas, and A. P. Minton, Macromolecular crowding and confinement: Biochemical, biophysical, and potential physiological consequences, *Annu. Rev. Biophys.* **37**, 375 (2008).
- [5] S. R. McGuffee and A. H. Elcock, Diffusion, crowding, and protein stability in a dynamic molecular model of the bacterial cytoplasm, *PLoS Comput. Biol.* **6**, e1000694 (2010).
- [6] G. Rivas and A. P. Minton, Macromolecular crowding in vitro, in vivo, and in between, *Trends Biochem. Sci.* **41**, 970 (2016).
- [7] P. M. Blanco, J. L. Garcés, S. Madurga, and F. Mas, Macromolecular diffusion in crowded media beyond the hard-sphere model, *Soft Matter* **14**, 3105 (2018).
- [8] A. Bhattacharya, Y. C. Kim, and J. Mittal, Protein-protein interactions in a crowded environment, *Biophys. Rev.* **5**, 99 (2013).
- [9] J. A. Dix and A. Verkman, Crowding effects on diffusion in solutions and cells, *Annu. Rev. Biophys.* **37**, 247 (2008).
- [10] D. S. Banks and C. Fradin, Anomalous diffusion of proteins due to molecular crowding, *Biophys. J.* **89**, 2960 (2005).
- [11] I. Pastor, E. Vilaseca, S. Madurga, J. L. Garcés, M. Cascante, and F. Mas, Diffusion of  $\alpha$ -chymotrypsin in solution-crowded media: A fluorescence recovery after photobleaching study, *J. Phys. Chem. B* **114**, 4028 (2010).
- [12] E. Vilaseca, I. Pastor, A. Isvoran, S. Madurga, J.-L. Garcés, and F. Mas, Diffusion in macromolecular crowded media: Monte Carlo simulation of obstructed diffusion vs. frap experiments, *Theor. Chem. Acc.* **128**, 795 (2011).
- [13] E. Vilaseca, A. Isvoran, S. Madurga, I. Pastor, J. L. Garcés, and F. Mas, New insights into diffusion in 3d crowded media by Monte Carlo simulations: Effect of size, mobility, and spatial distribution of obstacles, *Phys. Chem. Chem. Phys.* **13**, 7396 (2011).

- [14] J. Sun and H. Weinstein, Toward realistic modeling of dynamic processes in cell signaling: Quantification of macromolecular crowding effects, *J. Chem. Phys.* **127**, 155105 (2007).
- [15] P. Mereghetti and R. C. Wade, Atomic detail brownian dynamics simulations of concentrated protein solutions with a mean field treatment of hydrodynamic interactions, *J. Phys. Chem. B* **116**, 8523 (2012).
- [16] S. Kondrat, O. Zimmermann, W. Wiechert, and E. von Lieres, The effect of composition on diffusion of macromolecules in a crowded environment, *Phys. Biol.* **12**, 046003 (2015).
- [17] T. Sentjabrskaja, E. Zaccarelli, C. De Michele, F. Sciortino, P. Tartaglia, T. Voigtmann, S. U. Egelhaaf, and M. Laurati, Anomalous dynamics of intruders in a crowded environment of mobile obstacles, *Nat. Commun.* **7**, 11133 (2016).
- [18] I. Yu, T. Mori, T. Ando, R. Harada, J. Jung, Y. Sugita, and M. Feig, Biomolecular interactions modulate macromolecular structure and dynamics in atomistic model of a bacterial cytoplasm, *Elife* **5**, e19274 (2016).
- [19] P. M. Blanco, M. Via, J. L. Garcés, S. Madurga, and F. Mas, Brownian dynamics computational model of protein diffusion in crowded media with dextran macromolecules as obstacles, *Entropy* **19**, 105 (2017).
- [20] S. Smith and R. Grima, Fast simulation of Brownian dynamics in a crowded environment, *J. Chem. Phys.* **146**, 024105 (2017).
- [21] S. Bucciarelli, J. S. Myung, B. Farago, S. Das, G. A. Vliegthart, O. Holderer, R. G. Winkler, P. Schurtenberger, G. Gompfer, and A. Stradner, Dramatic influence of patchy attractions on short-time protein diffusion under crowded conditions, *Sci. Adv.* **2**, e1601432 (2016).
- [22] P.-h. Wang, I. Yu, M. Feig, and Y. Sugita, Influence of protein crowder size on hydration structure and dynamics in macromolecular crowding, *Chem. Phys. Lett.* **671**, 63 (2017).
- [23] R. Chakrabarti, S. Kesselheim, P. Košovan, and C. Holm, Tracer diffusion in a crowded cylindrical channel, *Phys. Rev. E* **87**, 062709 (2013).
- [24] A. Irbäck and S. Mohanty, Protein folding/unfolding in the presence of interacting macromolecular crowders, *Eur. Phys. J.: Spec. Top.* **226**, 627 (2017).
- [25] A. Stradner, H. Sedgwick, F. Cardinaux, W. C. Poon, S. U. Egelhaaf, and P. Schurtenberger, Equilibrium cluster formation in concentrated protein solutions and colloids., *Nature* **432**, 492 (2004).
- [26] A. Shukla, E. Mylonas, E. D. Cola, S. Finet, P. Timmins, T. Narayanan, and D. I. Svergun, Absence of equilibrium cluster phase in concentrated lysozyme solutions, *Proc. Natl. Acad. Sci. USA* **105**, 5075 (2008).
- [27] T. Lafitte, S. K. Kumar, and A. Z. Panagiotoulos, Self-assembly of polymer-grafted nanoparticles in thin films, *Soft Matter* **10**, 786 (2014).
- [28] T. Curk, F. J. Martinez-Veracoechea, D. Frenkel, and J. Dobnikar, Nanoparticle organization in sandwiched polymer brushes, *Nano Lett.* **14**, 2617 (2014).
- [29] G. Nie, G. Li, L. Wang, and X. Zhang, Nanocomposites of polymer brush and inorganic nanoparticles: Preparation, characterization, and application, *Polym. Chem.* **7**, 753 (2016).
- [30] D. Bedrov, C. Ayyagari, and G. D. Smith, Multiscale modeling of poly (ethylene oxide)-poly (propylene oxide)-poly (ethylene oxide) triblock copolymer micelles in aqueous solution, *J. Chem. Theory Comput.* **2**, 598 (2006).
- [31] D. Bedrov, G. D. Smith, and J. Yoon, Structure and interactions in micellar solutions: Molecular simulations of pluronic 164 aqueous solutions, *Langmuir* **23**, 12032 (2007).
- [32] N. Samanta and R. Chakrabarti, Tracer diffusion in a sea of polymers with binding zones: Mobile vs. frozen traps, *Soft Matter* **12**, 8554 (2016).
- [33] P. Kumar, L. Theeyancheri, S. Chaki, and R. Chakrabarti, Transport of probe particles in a polymer network: Effects of probe size, network rigidity and probe-polymer interaction, *Soft Matter* **15**, 8992 (2019).
- [34] C. N. Likos, H. Löwen, M. Watzlawek, B. Abbas, O. Jucknischke, J. Allgaier, and D. Richter, Star Polymers Viewed as Ultrasoft Colloidal Particles, *Phys. Rev. Lett.* **80**, 4450 (1998).
- [35] B. Loppinet, G. Fytas, D. Vlassopoulos, C. N. Likos, G. Meier, and G. J. Liu, Dynamics of dense suspensions of star-like micelles with responsive fixed cores, *Macromol. Chem. Phys.* **206**, 163 (2005).
- [36] L. Liu, W. K. den Otter, and W. J. Briels, Coarse grain forces in star polymer melts, *Soft Matter* **10**, 7874 (2014).
- [37] E. Locatelli, B. Capone, and C. N. Likos, Multiblob coarse-graining for mixtures of long polymers and soft colloids, *J. Chem. Phys.* **145**, 174901 (2016).
- [38] M. Quesada-Pérez, A. Moncho-Jordá, F. Martínez-Lopez, and R. Hidalgo-Álvarez, Probing interaction forces in colloidal monolayers: Inversion of structural data, *J. Chem. Phys.* **115**, 10897 (2001).
- [39] C. Contreras-Aburto, J. M. Méndez-Alcaraz, and R. Castañeda Priego, Structure and effective interactions in parallel monolayers of charged spherical colloids, *J. Chem. Phys.* **132**, 174111 (2010).
- [40] N. G. Almarza, J. Pękaliski, and A. Ciach, Periodic ordering of clusters and stripes in a two-dimensional lattice model. II. Results of Monte Carlo simulation, *J. Chem. Phys.* **140**, 164708 (2014).
- [41] J. R. Bordin, Distinct aggregation patterns and fluid porous phase in a 2D model for colloids with competitive interactions, *Physica A* **495**, 215 (2018).
- [42] A. Barros de Oliveira, P. A. Netz, T. Colla, and M. C. Barbosa, Thermodynamic and dynamic anomalies for a three-dimensional isotropic core-softened potential, *J. Chem. Phys.* **124**, 084505 (2006).
- [43] A. B. de Oliveira, P. A. Netz, T. Colla, and M. C. Barbosa, Structural anomalies for a three dimensional isotropic core-softened potential, *J. Chem. Phys.* **125**, 124503 (2006).
- [44] J. R. Bordin and M. C. Barbosa, Waterlike anomalies in a two-dimensional core-softened potential, *Phys. Rev. E* **97**, 022604 (2018).
- [45] L. B. Krott, N. Barraz, Jr., J. R. Bordin, and M. C. Barbosa, Effects of confinement on anomalies and phase transitions of core-softened fluids, *J. Chem. Phys.* **142**, 134502 (2015).
- [46] L. Krott and J. R. Bordin, Distinct dynamical and structural properties of a core-softened fluid when confined between fluctuating and fixed walls, *J. Chem. Phys.* **139**, 154502 (2013).
- [47] L. B. Krott, J. R. Bordin, and M. C. Barbosa, New structural anomaly induced by nanoconfinement, *J. Phys. Chem. B* **119**, 291 (2015).

- [48] P. A. Netz, F. W. Starr, M. C. Barbosa, and H. E. Stanley, Relation between structural and dynamical anomalies in supercooled water, *Physica A* **314**, 470 (2002).
- [49] T. Morishita, Anomalous diffusivity in supercooled liquid silicon under pressure, *Phys. Rev. E* **72**, 021201 (2005).
- [50] S. Sastry and C. A. Angell, Liquid-liquid phase transition in supercooled silicon, *Nat. Mater.* **2**, 739 (2003).
- [51] J. D. Weeks, D. Chandler, and H. C. Andersen, Role of repulsive forces in determining the equilibrium structure of simple liquids, *J. Chem. Phys.* **54**, 5237 (1971).
- [52] K. Kremer and G. S. Grest, Dynamics of entangled linear polymer melts: A molecular dynamics simulation, *J. Chem. Phys.* **92**, 5057 (1990).
- [53] A. Barros de Oliveira, E. Salcedo, C. Chakravarty, and M. C. Barbosa, Entropy, diffusivity and the energy landscape of a waterlike fluid, *J. Chem. Phys.* **132**, 234509 (2010).
- [54] R. Auhl, R. Everaers, G. S. Grest, K. Kremer, and S. J. Plimpton, Equilibration of long chain polymer melts in computer simulations, *J. Chem. Phys.* **119**, 12718 (2003).
- [55] M. P. Allen and D. J. Tildesley, *Computer Simulation of Liquids* (Oxford University Press, Oxford, 2017).
- [56] S. Plimpton, Fast parallel algorithms for short-range molecular dynamics, *J. Comput. Phys.* **117**, 1 (1995).
- [57] T. Ando and J. Skolnick, Crowding and hydrodynamic interactions likely dominate *in vivo* macromolecular motion, *Proc. Nat. Acad. Sci. USA* **107**, 18457 (2010).
- [58] G. G. Putzel, M. Tagliacuzzi, and I. Szleifer, Nonmonotonic Diffusion of Particles Among Larger Attractive Crowding Spheres, *Phys. Rev. Lett.* **113**, 138302 (2014).
- [59] S. S. L. Peppin, Theory of tracer diffusion in concentrated hard-sphere suspensions, *J. Fluid Mech.* **870**, 1105 (2019).
- [60] J. C. F. Toledano, F. Sciortino, and E. Zaccarelli, Colloidal systems with competing interactions: From an arrested repulsive cluster phase to a gel, *Soft Matter* **5**, 2390 (2009).
- [61] J. R. Bordin, Distinct self-assembly aggregation patterns of nanorods with decorated ends: A simple model study, *Fluid Phase Equilib.* **499**, 112251 (2019).
- [62] M. H. Holmes, Nonlinear ionic diffusion through charged polymeric gels, *SIAM J. Appl. Math.* **50**, 839 (1990).
- [63] U. Yamamoto and K. S. Schweizer, Theory of nanoparticle diffusion in unentangled and entangled polymer melts, *J. Chem. Phys.* **135**, 224902 (2011).
- [64] K. N. Pham, A. M. Puertas, J. Bergenholtz, S. U. Egelhaaf, A. Moussaid, P. N. Pusey, A. B. Schofield, M. E. Cates, M. Fuchs, and W. C. K. Poon, Multiple glassy states in a simple model system, *Science* **296**, 104 (2002).
- [65] J. Kurzidim and G. Kahl, Accessible volume in quenched-annealed mixtures of hard spheres: A geometric decomposition, *Mol. Phys.* **109**, 1331 (2011).
- [66] J. Kurzidim, D. Coslovich, and G. Kahl, Impact of random obstacles on the dynamics of a dense colloidal fluid, *Phys. Rev. E* **82**, 041505 (2010).